Symmetry breaking effects of density gradient on parallel momentum transport: A new ρ_s^* effect

Rameswar Singh,[1,a)] R. Singh,[1] P. Kaw,[1] Ö. D. Gürcan,[2] P. H. Diamond,[3] and H. Nordman[4]
[1]*Institute for Plasma Research, Bhat, Gandhinagar 382 428, India*
[2]*Laboratoire de Physique des Plasmas, Ecole Polytechnique, CNRS, 91128 Palaiseau Cedex, France*
[3]*Center for Astrophysics and Space Sciences, University of California, San Diego, 9500 Gilman Dr., La Jolla, California 92093-0424, USA*
[4]*Department of Earth and Space Sciences, Chalmers University of Technology, SE-412 96 Göteborg, Sweden*

(Received 10 October 2011; accepted 18 November 2011; published online 6 January 2012; publisher error corrected 18 January 2012)

Symmetry breaking effects of density gradient on parallel momentum transport is studied via quasilinear theory. It is shown that finite $\rho_s^*(\equiv \rho_s/L_n)$, where ρ_s is ion sound radius and L_n is density scale length, leads to symmetry breaking of the ion temperature gradient (ITG) eigenfunction. This broken symmetry persists even in the absence of mean poloidal (from radial electric field shear) and toroidal flows. This effect, as explained in the text, originates from the divergence of polarization particle current in the ion continuity equation. The form of the eigenfunction allows the microturbulence to generate parallel residual stress via $\langle k_\parallel \rangle$ symmetry breaking. Comparison with the $\vec{E} \times \vec{B}$ shear driven parallel residual stress, parallel polarization stress and turbulence intensity gradient driven parallel residual stress are discussed. It is shown that this ρ_s^* driven parallel residual stress may become comparable to $\vec{E} \times \vec{B}$ shear driven parallel residual stress in small L_n region. In the regular drift wave ordering, where $\rho_s^* \ll 1$, this effect is found to be of the same order as the parallel polarization stress. This ρ_s^* driven parallel residual stress can also overtake the turbulence intensity gradient driven parallel residual stress in strong density gradient region whereas the later one is dominant in the strong profile curvature region. The parallel momentum diffusivity is found to remain undisturbed by this ρ_s^* effect as long as the turbulence intensity inhomogenity is not important. © *2012 American Institute of Physics*. [doi:10.1063/1.3672518]

I. INTRODUCTION

Intrinsic rotation in tokamak plasmas is a subject which attained considerable recent popularity. It is an interesting problem linked to turbulent momentum transport and the transition from low (L) to high (H) confinement modes, whose study is of key importance for an understanding of tokamak operation. This is true, in particular because rotation plays an important (if not key) role in the L-H transition. The threshold power for L-H transition depends strongly on the toroidal rotation level.[1] Mean $E \times B$ shear, be it self-generated like zonal flow shear or by external radial electrode biasing, is well known to suppress turbulence.[2–5] Toroidal rotation couples dynamically to the $E \times B$ shear and thus affects the turbulence suppression mechanism, which is believed to be important for the L-H transition as well as the formation of internal transport barriers (ITBs).[6] Toroidal rotation is also helpful in suppressing certain types of harmful magnetohydrodynamic (MHD) instabilities, such as resistive wall modes (RWM) (Refs. 7–10) whose stability is a major concern for advanced ITER scenerios.[11] RWMs are nothing but the long wavelength MHD kink modes in the presence of a resistive wall. RWMs stability can facilitate tokamaks to operate at normalized pressure values beyond the no-wall stability limit and rotation plays a significant role in achieving this. In current generation tokamaks, neutral beam injection (NBI) is the main external driver of rotation. However, use of NBI in ITER and other future reactor scale machines to achieve desired rotation is still debatable because of unvoidable bulky size of these machines.[12–14] Hence, self generated rotation will play a vital role in suppression of RWMs. Fortunately Rice scaling predicts a toroidal intrinsic rotation Alfven Mach number of $M_A \geq 0.02$ for ITER plasma and that appears to be sufficient for stabilization of RWMs.[15] This suggests that the RWMs in the ITER plasma will probably be self-stabilized because of spontaneous rotation itself, which would provide an alternative solution to the NBI problem apart from the active feedback control of RWMs.[11] These findings have sparked extensive theoretical and experimental studies on intrinsic rotation generation.

While the intrinsic rotation (or rather the intrinsic spin-up during the L-H transition) was discovered experimentally in a database study[15,16] and observed in various machines (e.g., see Ref. 17 for a comprehensive review of recent experimental results) in almost all modes of discharges, consequent theoretical efforts (e.g., Ref. 18 and references therein) has lead to a certain understanding of the phenomenon mostly as a

a)Electronic mail: rameswar@ipr.res.in.

self-organization process linked to the L-H transition. It is understood for instance, that a breaking of the symmetry of the underlying microturbulence is necessary in order for the turbulence to generate a net wave-momentum, whose flux is then tied to the transport of the bulk plasma momentum.[19] In addition to a diffusive component, the plasma momentum flux, consists of two separate kinds of off-diagonal pieces. The diffusive momentum flux has been studied extensively both theoretically[20,21] and experimentally[22] and established momentum diffusivity $\chi_\phi \sim \chi_i$, ion thermal diffusivity except with some departure from this scaling noted in recent gyrokinetic simulation.[23] The effects of curvature in a tokamak, result in a pinch-like contribution,[24–28] mainly via a turbulent equipartition (TEP) mechanism.[26] While this term transports momentum (especially when the rotation is already sufficiently large), its effect on rotation itself is not too pronounced. In contrast a residual stress term can be driven by various different mechanisms including Alfven waves,[29] intensity gradients,[30],up-down asymmetry of current[31,32] and toroidicity.[33] And the residual stress due to a self-consistent $E \times B$ shear that feedback from the pressure gradient through the radial force balance is a possible mechanism that may explain the intrinsic L-H spin-up.[34] Experiments on JT-60U by Yoshida *et al.*[35] also seem to support this pressure gradient scaling. However, the discovery of I mode,[36] where particle transport is like L mode and energy transport is like H mode, and a recent follow up experiment by Rice *et al.*[37] in Alcator C-Mod suggests that gradient in temperature rather than gradient in pressure is the main driver of intrinsic rotation. Experiments on the large helical device (LHD) with ITB also demonstrate temperature gradient as the driver of toroidal intrinsic roatation.[38] Recent gyro-kinetic simulations,[21,39,40] have verified certain aspects of mean $E \times B$ shear driven mechanism and also highlighted the role of the intensity gradient[30] as a mechanism for driving residual stress. Wang *et al.*,[39,41] in gyrokinetic simulations, have also demonstrated nonlinear residual stress generation in collisionless trapped electron mode turbulence. The fundamental similarity underlying all the above mentioned residual stress generation mechanisms is the symmetry breaking in $k_\parallel$ (i.e., $\langle k_\parallel \rangle \neq 0$ where $\langle\rangle$ indicates average over fluctuation spectrum) by macroscopic gradients. Different means of breaking $\langle k_\parallel \rangle$ symmetry has lead to different mechanisms of residual stress generation. For example, $\langle k_\parallel \rangle$ symmetry breaking by asymmetrizing the eigenfunction via mean $E \times B$ shear.[34,42] A fundamentally different mechanism of residual stress generation based on $\langle k_\parallel k_x \rangle$ symmetry breaking has also been shown to be driven by polarization drift[42–44] which does not require asymmetry in eigenfunction. The residual stress is the key driver of intrinsic rotation be it toroidal or azimuthal.[42] The connection between azimuthal intrinsic rotation and directly measured azimuthal residual stress has been demonstrated by Yan *et al.*[45] in Controlled Shear Decorrelation Experiment (CSDX) plasmas. The residual stress combined with proper boundary condition can explain intrinsic spin-up of the core. However, a recent experiment[46] shows that all the features of intrinsic rotation cannot be explained just by fluid turbulent stresses.

While the effect of temperature gradient seems to be more pronounced on the experimental observations of intrinsic rotation. The density gradient can also generate residual stress. Furthermore, the mechanism for the generation of this residual stress is more direct, and the symmetry breaking is more general in the case of drift waves. Here, we will discuss the effect of finite ρ_s^*, and show that the ion temperature gradient (ITG) eigenmode has a broken symmetry in the case of sharp density gradients (e.g., as in an H-mode).

The analytical derivation presented in this paper is performed in simple slab geometry. This is considered as a local piecewise linear approximation to a small part of the plasma in the vicinity of the low field side of the tokamak. While this approach does not capture the exact form of the eigenmode it represents the local processes as long as the microturbulence is sufficiently small scale with their eigenmodes tightly packed.

The process that leads to symmetry breaking due to finite ρ_s^*, arises from the well known expression for the divergence of polarization current, which enter the quasi-neutrality equation in the usual dimensionless units (i.e., $x \to x/\rho_i$, $\phi \to e\Phi/T_i$, etc.) as

$$\nabla_\perp \cdot \left[n \frac{D}{Dt} \vec{\nabla}_\perp \phi \right] + \nabla_\parallel J_\parallel = 0,$$

while part of the above perpendicular divergence gives rise to the usual definition of vorticity, part of it leads to a nonlinear term which survives in the linear limit due to the existence of the background density gradient. This term is normally small since it involves both the density gradient and the D/Dt, (and for drift waves $D/Dt \sim \omega_*$ already). However, it can become important when the background flow is sufficiently large (i.e., $V_0 k > \omega_*$) or if the density gradient is sufficiently large (i.e., an H-mode pedestal for instance). Physically, this term comes from the fluctuating radial gradient of the polarization current that arise from the radial gradient of the density of the particles that generate this fluctuating current (by their fluctuating polarization drift motions). We will show that the inclusion of this term in the ITG eigenmode calculation, leads to a symmetry breaking in $k_\parallel$, and therefore, a net non-zero momentum flux, which has in principle the form of a residual stress. To justify further the importance of this effect, we show the comparisons of this with the residual stresses driven by E_r-shear, parallel polarization residual stress and the intensity gradient. It is shown that for fixed E_r-shear the ρ_s^* induced residual stress may become comparable to E_r-shear driven residual stress in the region of small L_n. ρ_s^* induced residual stress turns out to be of the same order as the parallel polarization stress in the regular drift wave ordering where $\rho_s^* \sim \omega/\omega_{ci} \ll 1$, ω is typical mode frequency and ω_{ci} is the ion gyro frequency. And comparison with turbulence intensity gradient driven residual stress shows that ρ_s^* driven residual stress dominates at the sharp density gradient region whereas the intensity gradient driven residual stress dominates at the strong profile curvature regions such as head and the foot of the ITB or the H-mode pedestal.

The rest of the paper is organized as follows. In Sec. II, we start with the derivation of a simple set of reduced fluid equations, and continue with deriving an eigenmode equation corresponding to this system. In the final part of the Sec. II, we present the solution of this eigen-mode equation, which displays a characteristic shift from the mode rational surface on which it is localized. In Sec. III, we discuss the

effect of this mode shift on momentum transport via the symmetry breaking mechanism, and compare this with the effect due to $E \times B$ shear, parallel polarization stress and the turbulence intensity gradient driven residual stress. We conclude and discuss the implications of our work in Sec. IV.

II. RADIAL EIGENMODE ANALYSIS

In this section, the linear eigenfunction for electrostatic ITG instability in the presence of mean flows is derived. A simplified set of fluid equations that describes the ion temperature gradient driven instability in the electrostatic regime is derived in the presence of poloidal and toroidal sheared flows. The assumptions made are (1) quasineutrality $\delta\tilde{n}_e = \delta\tilde{n}_i$, (2) constant electron temperature, (3) zero resistivity, (4) zero electron inertia for $c_i \leq \frac{\omega}{k_\parallel} < c_e$, and (5) $\omega \ll \omega_{ci}$, where $c_{i,e} = \sqrt{\frac{T_{0i,e}}{m_{i,e}}}$ is the ion(i)/electron(e) thermal speed, $T_{0i,e}$ are ion(i)/electron(e) temperatures, $m_{i,e}$ is ion/electron mass, ω is a typical frequency, $\omega_{ci} = \frac{eB}{m_i}$ is ion cyclotron frequency and $\eta_i = \frac{L_n}{L_{T_i}}$ is the ratio of density and ion temperature scale lengths, $L_n^{-1} = -\frac{d\ln n_0}{dx}$ and $L_{T_{si}}^{-1} = -\frac{d\ln T_{i0}}{dx}$, respectively. For concreteness, we closely follow the Ref. 42. We use $(x, y.z)$ orthogonal Cartesian coordinate system, with unit vectors $\hat{x}, \hat{y}, \hat{z}$, situated at a rational surface. All the equilibrium quantities are considered to vary in x direction only. We consider a sheared slab configuration of magnetic field $\vec{B}$ in the neighborhood of a rational surface situated at x_0

$$\vec{B} = B(\hat{z} + \frac{x - x_0}{L_s}\hat{y}), \tag{1}$$

where $L_s^{-1} = \frac{B'_y}{B}$ is magnetic shear scale length. We also consider a mean ion flow field $\vec{V}_{i0}$ lying in the (x, y) plane. For fluctuations localized on a particular rational surface at $x = x_0$, the mean ion flow velocity may be expanded as

$$\vec{V}_{i0}(x) = \vec{V}_{i0}(x_0) + (x - x_0)\left(\frac{\partial \vec{V}_{i0}}{\partial x}\right) + \ldots. \tag{2}$$

We will describe the system of equations in inertial frame moving with constant velocity $\vec{V}_{i0}(x_0)$. The perturbed linearized continuity, momentum and pressure equations for ions can be obtained as

$$\left(\frac{\partial}{\partial t} + x\hat{V}'_{E0}\nabla_y\right)(1 - \nabla_\perp^2 + \rho_s^*\nabla_x)\phi + \left[1 + K\left(\nabla_\perp^2 - \rho_s^*\nabla_x\right)\right]\nabla_y\phi + \nabla_\parallel v = 0, \tag{3}$$

$$\left(\frac{\partial}{\partial t} + x\hat{V}'_{E0}\nabla_y\right)v - \hat{V}'_{\parallel 0}\nabla_y\phi + \nabla_\parallel(p + \phi) = 0, \tag{4}$$

$$\left(\frac{\partial}{\partial t} + x\hat{V}'_{E0}\nabla_y\right)p + K\nabla_y\phi + \Gamma\nabla_\parallel v = 0, \tag{5}$$

where normalizations are chosen such that $x = (x - x_0)/\rho_s$, $y = y/\rho_s$, $z = z/L_n$, $t = tc_s/L_n$, $\phi = (e\delta\phi/T_e)(L_n/\rho_s)$, $n_i = (\delta n_i/n_0)(L_n/\rho_s)$ $v = (\delta v_{\parallel i}/c_s)(L_n/\rho_s)$, $p = (\tau_i\delta p_i/P_{i0})(L_n/\rho_s)$, $L_n\nabla_\parallel \equiv \nabla_\parallel = \frac{\partial}{\partial z} + xs\frac{\partial}{\partial y}$ with the nondimensional parameters: $\eta_i = L_n/L_T$, $K = \tau_i(1 + \eta_i) = \tau_i\alpha_i$, $\tau_i = T_{0i}/T_{0e}$, $\Gamma = \gamma\tau_i$, $s = L_n/L_s$, $\hat{V}'_{E0} = (L_n/c_s)V'_{E0}$, $\hat{V}'_{\parallel 0} = (L_n/c_s)V'_{\parallel 0}$, $\rho_s = c_s/\omega_{ci}$, and $\rho_s^* = \rho_s/L_n$. The difference between the above set of linear equations and that obtained in the past Refs. 42 and 47–49, etc., is in the ion continuity Eq. (3) which now contains an additional term proportional to ρ_s^*. However, Dubin *et al.*[50] has retained such term in their gyrokinetic formulation to ensure energy conservation. This term arises from the density gradient dependent part $\vec{V}_{pol}\cdot\vec{\nabla}n_0$ of the divergence of ion polarization current density $\vec{\nabla}\cdot(n_0\vec{V}_{pol})$. As can be obviously seen in the Eq. (3), this term is one order higher in ρ_s^* in the regular drift wave ordering scheme, and hence, it is normally not considered in drift wave theory. But it is clear that this term can become significant in strong particle density gradient regions such as in the H-mode pedestal. Also, the above set of fluid equations are in fact a subset of the general gyro-fluid system of equations, which can also be derived by taking the moments of the gyro-kinetic equation.[51] The effect of this ρ_s^* term on the eigenmode structure is derived in the following. We consider the perturbation of the form $f = f_k(x)exp(ik_y y - i\omega t)$, where k_y and ω are normalized as $k_y = k_y\rho_s, \omega = \omega/(c_s/L_n)$, the above set of Eqs. (3)–(5) form an eigenvalue problem in the x direction for the Fourier amplitude ϕ_k

$$\frac{d^2\phi_k}{dx^2} - \rho_s^*\frac{d\phi_k}{dx} + \left[-k_y^2 + \frac{k_y - \omega}{\tau_i\alpha_i k_y + \omega - xk_y\hat{V}'_{E0}} + k_y^2\frac{(sx)^2}{(\omega - xk_y\hat{V}'_{E0})^2 - \Gamma(sx)^2}\right]\phi_k + xk_y\left[\frac{\hat{V}'_{E0}}{\tau_i\alpha_i k_y + \omega - xk_y\hat{V}'_{E0}} - \frac{\hat{V}'_{\parallel 0}}{(\omega - xk_y\hat{V}'_{E0})(\tau_i\alpha_i k_y + \omega - xk_y\hat{V}'_{E0})}\right]\phi_k = 0. \tag{6}$$

For shearing rate is much smaller than the mode frequency, Eq. (6) simplifies to

$$\frac{d^2\phi_k}{dx^2} - \rho_s^*\frac{d\phi_k}{dx} + \left[-k_y^2 + \frac{k_y - \omega}{\tau_i\alpha_i k_y + \omega} + k_y^2\frac{(xs)^2}{\omega^2} + xk_y\left[\frac{\hat{V}'_{E0}}{\tau_i\alpha_i k_y + \omega} - \frac{\hat{V}'_{\parallel 0}}{\omega(\tau_i\alpha_i k_y + \omega)}\right]\right]\phi_k = 0, \tag{7}$$

which can be written as

$$\frac{d^2\phi_k}{dx^2} - \rho_s^*\frac{d\phi_k}{dx} + (A_1 + A_2 x + A_3 x^2)\phi_k = 0, \tag{8}$$

where

$$A_1 = \frac{k_y - \omega}{\tau_i\alpha_i k_y + \omega} - k_y^2, A_2 = \frac{k_y}{\tau_i\alpha_i k_y + \omega}\left(\hat{V}'_{E0} - k_y s\frac{\hat{V}'_{\parallel 0}}{\omega}\right), \quad A_3 = \left(\frac{k_y s}{\omega}\right)^2. \tag{9}$$

The total eigen function satisfying Eq. (8) for the $l = 0$ radial quantum number, can be obtained as

$$\phi_k = \Phi_0 \exp\left[-\frac{1}{2} i\sqrt{A_3}\left(x + \frac{A_2}{2A_3}\right)^2\right] \exp\left[\frac{1}{2}\rho_s^*\left(x + \frac{A_2}{2A_3}\right)\right], \tag{10}$$

and the corresponding eigenmode dispersion relation is

$$\omega^2(1 + k_y^2) + \omega(k_y(-1 + k_y^2\tau_i\alpha_i) + is|k_y|) + is\tau_i\alpha_i k_y|k_y| = -\frac{\omega k_y^2\left[\frac{\omega}{sk_y}\hat{V}'_{E0} - \hat{V}'_{\|0}\right]^2}{4(\tau_i\alpha_i k_y + \omega)} - \frac{1}{4}\rho_s^{*2}\omega(\tau_i\alpha_i k_y + \omega). \tag{11}$$

Equation (10) shows that the eigenfunction is shifted off the mode rational surface, even in the absence of background shear flows, due to finite ρ_s^*. In the absence of shear flows, the above equation becomes

$$\phi_k = \Phi_0 \exp\left[-\frac{1}{2}\left(\frac{x - \xi_{*k}}{\Delta_k}\right)^2\right] \exp\left[-i\frac{1}{2}Re\sqrt{A_3}x^2\right], \tag{12}$$

where a factor of $\exp(-\rho_s^{*2}/2Im\sqrt{A_3})$ has been absorbed in the amplitude Φ_0. Mode width $\Delta_k^{-2} = -Im\sqrt{A_3} = |k_y|s\gamma/|\omega|^2$ and mode shift off the rational surface is $\xi_{*k} = -\rho_s^*/2Im\sqrt{A_3} = \rho_s^*|\omega|^2/(2|k_y|s\gamma) = \rho_s^*\Delta_k^2/2$. Also the real part of the radial wave number is $Re(k_x) = -\frac{1}{2}Re\sqrt{A_3}x$ and $\omega = \omega_r + i\gamma$.

From dispersion relation, Eq. (11) one can pick up a slow mode, on the low k_y side of the spectrum, as

$$\omega = \frac{is\tau_i\alpha_i|k_y|}{1 - k_y^2\tau_i\alpha_i - (1/4)\rho_s^{*2}\tau_i\alpha_i} \approx is\tau_i\alpha_i|k_y|. \tag{13}$$

The dispersion relation Eq. (11) is rewitten in a form where the frequency is normalized by c_s/R and L_s is written as $L_s = qR(1/\hat{s})$. Here, R is the tokamak major radius, $\hat{s} = rq'/q$ is the shear in safety factor q. The resulting dispersion relation with $\hat{V}'_{E0} = \hat{V}'_{\|0} = 0$ is solved numerically using the MATLAB root finding routines. Fig. 1 shows the plots of real frequency and growth rates vs k_y. Next, we computed the eigenfunction Eq. (10) for the highest growth rate. Fig. 2 shows the shift of eigenmode structure off the mode rational surface without mean flows.

III. MOMENTUM FLUX BY REYNOLDS STRESSES

The net radial flux of parallel momentum $\langle nv_r v_\| \rangle$ is broadly composed of particle flux driven momentum flux $\langle v_\| \rangle \langle \delta n \delta v_r \rangle$, Reynolds stress driven momentum flux $\langle n \rangle \langle \delta v_r \delta v_\| \rangle$ and mean radial flow driven momentum flux $\langle v_r \rangle \langle \delta n \delta v_\| \rangle$ and triple correlation $\langle \delta n \delta v_r \delta v_\| \rangle$. Since particle flux vanishes for adiabatic electron response and there are no mean radial flows, in this section, we calculate the momentum flux due to parallel Reynolds stress carried by fluctuating $E \times B$ drift. We first compute the flux driven by only ρ_s^* induced symmetry breaking of the eigenfunction. Then, in the subsequent subsections comparisons are made with E_r shear induced symmetry breaking driven residual stress, parallel

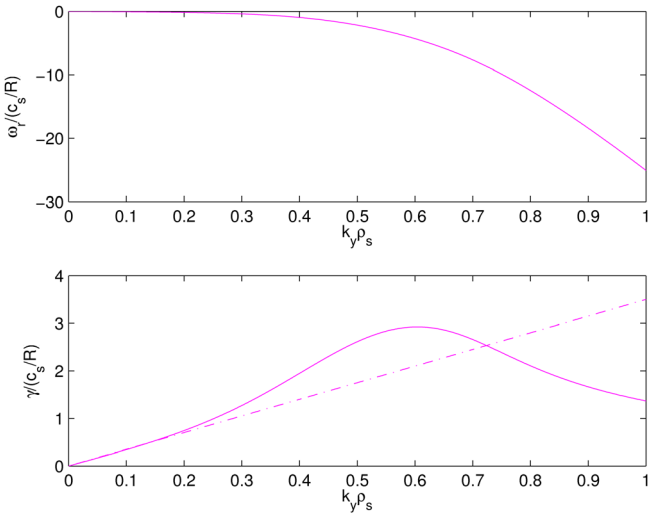

FIG. 1. (Color online) Real frequencies (a) and growth rates (b) vs k_y obtained from numerical solution of the dispersion relation. The dashed-dotted (-.-.-. curve) represents the analytical approximation of the growth rate on the low k_y side of the spectrum only. Parameters: $L_n = 0.05$ m, $L_T = 0.020$ m, $\hat{s} = 2.0$, $q_{a/2} = 2.0$, $R = 1$ m, $a = 0.25$ m, $T_e = T_i = 4$ KeV, $m_i = 1.6 \times 10^{-27}$ Kg, $B = 4.6$ T, $r = a/2$.

polarization stress and turbulence intensity gradient induced symmetry breaking driven residual stress, respectively, to gain a feeling for the importance of the new effect reported here. From Eqs. (4) and (5), we get the parallel velocity response as

$$\delta v_{\|,k} = \left(\frac{c_s\rho_s}{L_n}\right)\frac{k_y}{\omega}\left[-\hat{V}'_{\|0} + \frac{k_\|}{k_y}\left[1 - \frac{\omega_{*pi}}{\omega}\right]\right]\phi_k. \tag{14}$$

The parallel Reynolds stress due to fluctuating $E \times B$ drift, using Eq. (14) for the parallel velocity fluctuation response, is obtained as

$$\langle \delta v_{Ex}\delta v_\| \rangle = Re\left(\frac{c_s\rho_s}{L_n}\right)^2 \sum_{\vec{k}} i\frac{k_y^2}{\omega}\left[-\hat{V}'_{\|0} + \frac{k_\|}{k_y}\left[1 - \frac{\omega_{*pi}}{\omega}\right]\right]|\phi_k|^2, \tag{15}$$

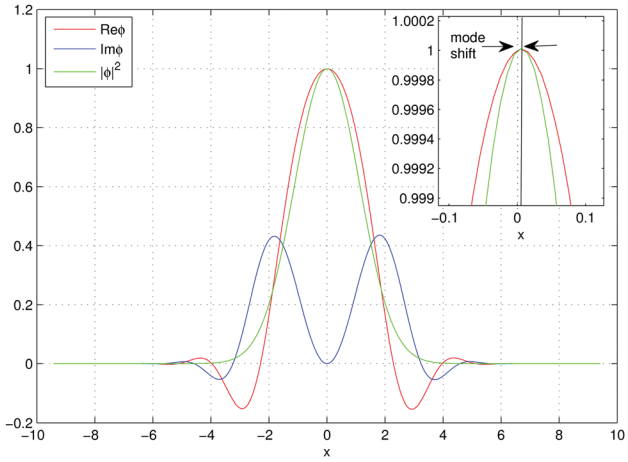

FIG. 2. (Color online) Eigenfunction shifts off the resonant surface due to finite ρ_s^*. The figure shows $Re\phi$ (— curve), $Im\phi$ (— curve) and $|\phi|^2$ (— curve). The zoomed-in subplot highlights the mode shift. The solid vertical line indicates the peak of the shifted eigenfunction. Parameters: $k_{y,max} = 0.60$, $\gamma_{max} = 2.92$, $\omega_{r,max} = -4.41$, and other parameters are same as in Fig. 1. The mode width is $\Delta = 1.59$, the mode shift is $\xi = 5.9 \times 10^{-03}$ and the mode averaged $\langle k_\| \rangle = 3.15 \times 10^{-03}$.

where $\langle ... \rangle$ indicates averaging over fast space-time scale. From above Eq. (15), the diffusive parallel momentum flux is

$$\Pi^{diff}_{\parallel,x} = mn_0 \langle \delta v_{Ex} \delta v_\parallel \rangle_{diff} = -\chi_\parallel mn_0 \frac{dV_\parallel}{dx}, \tag{16}$$

where the diffusivity is given by

$$\chi_\parallel = \left(\frac{c_s\rho_s}{L_n}\right)^2 \sum_{k_y} k_y^2 \frac{\sqrt{\pi}}{\Delta_k} \frac{L_n}{c_s} |\phi_{0k}|^2. \tag{17}$$

The residual flux is given by

$$\Pi^{res}_{\parallel,x} = mn_0 \langle \delta v_{Ex} \delta v_\parallel \rangle_{res} = mn_0 \left(\frac{c_s\rho_s}{L_n}\right)^2 \sum_{\vec{k}} k_y k_\parallel \left[\frac{\gamma}{|\omega|^2} + \frac{\omega_{*pi} 2\gamma\omega_r}{|\omega^2|^2}\right] |\phi_k|^2. \tag{18}$$

For the particular slow mode, Eq. (13), where $\omega_r = 0$, the above residual flux expression becomes

$$\Pi^{res}_{\parallel,x} = mn_0 \left(\frac{c_s\rho_s}{L_n}\right)^2 \sum_{k_y} k_y |k_y| s \frac{\gamma}{|\omega|^2} \langle k_\parallel \rangle, \tag{19}$$

where the spectrum average of $k_\parallel$ is defined as

$$\langle k_\parallel \rangle = \langle k_\parallel |\phi_k|^2 \rangle_x, \tag{20}$$

where we have made use of $\sum_{\vec{k}} (\cdots) = \sum_{k_y} |k_y| s \langle (\cdots) \rangle_x = \sum_{k_y} |k_y| s \int_{-\infty}^{+\infty} dx (\cdots)$ to evaluate the summation over $\vec{k}$ for tightly packed modes. Further using $k_\parallel = k_y s x$ and $\langle x|\phi_k|^2 \rangle_x = \xi_{*k} \Delta_k \sqrt{\pi} |\phi_{0k}|^2$ gives the parallel residual flux as

$$\Pi^{res}_{\parallel,x} = mn_0 \left(\frac{c_s\rho_s}{L_n}\right)^2 \sum_{k_y} \frac{1}{2} k_y^2 \rho_s^* s \Delta_k \sqrt{\pi} |\phi_{0k}|^2. \tag{21}$$

This clearly shows parallel residual flux generation due to finite ρ_s^* effect. The parallel residual flux to parallel diffusivity ratio is

$$\frac{\Pi^{res}_{\parallel,x}}{\chi_\parallel} = mn_0 s \frac{c_s}{L_n} \frac{\langle x|\phi_k|^2 \rangle_x}{\langle |\phi_k|^2 \rangle_x} = mn_0 s \xi_{*k} \frac{c_s}{L_n} = \frac{1}{2} mn_0 s \frac{c_s}{L_n} \rho_s^* \Delta_k^2. \tag{22}$$

This demonstrates parallel mean flow generation via microturbulence due to finite ρ_s^* effect.

A. Comparison with fluxes driven by mean radial electric field shear

Following Ref. 42 the slow mode eigenfunction, with mean $E \times B$ shear present and ignoring the ρ_s^* term, is given by

$$\phi_k^E = \phi_{0ks} \exp\left[-\frac{1}{2}\left(\frac{x - \xi_{Ek}}{\Delta_{ks}}\right)^2\right] \exp\left[i \frac{|k_y|}{k_y} \frac{\hat{V}'_{\parallel 0}}{2\tau_i\alpha_i} x\right], \tag{23}$$

where $\xi_{Ek} = \Delta_{ks}^2 \hat{V}'_{E0}/2$ and $\Delta_{ks}^2 = \tau_i\alpha_i$. Note that here we correctly obtained the factor $|k_y|/k_y$ in the complex exponent in the Eq. (23) which was missing in the Ref. 42. The slow mode frequency turns out to be

$$\omega = is\tau_i\alpha_i |k_y| \tag{24}$$

In the above and in the following equations, the subscript or superscript E indicates corresponding quantities with mean $E \times B$ shear only. Using Eqs. (15), (23), and (24), as shown in Eq. (48) of Ref. 42, the parallel momentum diffusivity $\chi_\parallel^E$ is given by

$$\chi_\parallel^E = \left(\frac{c_s\rho_s}{L_n}\right)^2 \sum_{k_y} k_y^2 \frac{\sqrt{\pi}}{\Delta_{ks}} \frac{L_n}{c_s} |\phi_{0ks}|^2, \tag{25}$$

and the parallel residual momentum flux $\Pi^{E,res}_{\parallel,x}$ can be written in the form

$$\Pi^{E,res}_{\parallel,x} = mn_0 \left(\frac{c_s\rho_s}{L_n}\right)^2 \sum_{k_y} k_y |k_y| s \frac{\gamma}{|\omega|^2} \langle k_\parallel \rangle_E, \tag{26}$$

where

$$\langle k_\parallel \rangle_E = k_y s \langle x|\phi_k^E|^2 \rangle_x = k_y s \xi_{Ek} \Delta_k \sqrt{\pi} |\phi_{0k}|^2, \tag{27}$$

and $\xi_{Ek} = \Delta_{ks}^2 \hat{V}'_{E0}/2$. Plugging the above form of $\langle k_\parallel \rangle_E$ and the mode frequency, Eq. (24) gives the form of the residual stress as obtained in the Ref. 42

$$\Pi^{E,res}_{\parallel,x} = mn_0 \left(\frac{c_s\rho_s}{L_n}\right)^2 \sum_{k_y} k_y^2 s \xi_{ks} \sqrt{\pi}/\Delta_{ks} |\phi_{0ks}|^2. \tag{28}$$

Comparing Eqs. (17) and (25), we get

$$\frac{\chi_\parallel}{\chi_\parallel^E} = 1. \tag{29}$$

That is the parallel momentum diffusivity remains unaltered. This is because the summand in the Eq. (17) contains $|\phi_k|^2$ and no other multiples of function of x. Eigenfunction symmetry breaking has no role in determining parallel diffusivity $\chi_\parallel$ as long as the turbulence intensity is homogenous. Again from Eqs. (21) and (26), we get

$$\frac{\Pi^{res}_{\parallel,x}}{\Pi^{E,res}_{\parallel,x}} = \frac{\langle k_\parallel \rangle}{\langle k_\parallel \rangle_E} = \frac{\rho_s^*}{\hat{V}'_{E0}}. \tag{30}$$

Here, we have made use of $\Delta_{ks} = \Delta_k$ because the mode width is determined by $\sqrt{A_3}$ which is the same in both cases of the momentum flux calculation. Equation (30) suggests that ρ_s^* induced $\langle k_\parallel \rangle$ symmetry breaking driven residual flux may become comparable to E_r-shear induced $\langle k_\parallel \rangle$ symmetry breaking driven residual flux in strong density gradient regions such as ITB and pedestal in H-mode plasma.

Note that a similar result is expected if one considers the zonal $E \times B$ shear as a source of symmetry breaking, since in a quasi-steady state, the zonal flow shear level can be roughly determined by the balance of zonal shear frequency

V'_{E0} with linear growth rate γ, (that is $V'_{E,ZF} \approx \gamma \propto \rho_s^*$). This means that the ρ_s^* effect introduced here can be viewed as linked to the zonal $E \times B$ shear induced symmetry breaking mechanism.

In a more rigorous computation of the Zonal Flow (ZF) shear driven residual stress, since the screening length of the ZF would be proportional to the poloidal gyro-radius the effect would probably be more pronounced. A quick way to realize this fact is as follows. $\hat{V}'_{E0}$ may result from the Rosenbluth Hinton (R H) neoclassical residual zonal flow.[52] The corresponding potential is

$$\frac{e\phi}{T_i} = \frac{1}{1 + 1.6q^2/\epsilon^{1/2}} \int dt S_{ik} / \left(k_\perp^2 a_i^2\right), \tag{31}$$

where $\epsilon = r/R$, running minor radius and $a_i^2 = (T_i/m_i)/\omega_{ci}^2$. Now, we estimate the $\hat{V}'_{E0}$, the $E \times B$ shear required for asymmetric eigenfunction as follows:

$$\hat{V}'_{E0} = \frac{L_n}{c_s} V'_{E0} \approx \frac{L_n}{c_s} \frac{1}{L_\phi^2} c_s \rho_s \left(\frac{e\phi}{T_e}\right), \tag{32}$$

where L_ϕ is potential scale length. We assume $\int dt S_{ik} / \left(k_\perp^2 a_i^2\right) = 1$. Then, the ratio of ρ_s^* induced residual stress to $E \times B$ shear driven residual stress becomes

$$\frac{\Pi_{\parallel,x}^{res}}{\Pi_{\parallel,x}^{E_{R.H},res}} = \frac{\rho_s^*}{\hat{V}'_{E0}} = \frac{L_\phi^2}{L_n^2} \frac{1}{(e\phi/T_e)} = \frac{L_\phi^2}{L_n^2} \frac{\left(1 + 1.6q^2/\epsilon^{1/2}\right)}{\tau_i}, \tag{33}$$

where $\tau_i = T_i/T_e$. In neoclassical theory $L_n \sim L_\phi$, therefore

$$\frac{\Pi_{\parallel,x}^{res}}{\Pi_{\parallel,x}^{E_{R.H},res}} = \frac{\left(1 + 1.6q^2/\epsilon^{1/2}\right)}{\tau_i} > 1. \tag{34}$$

This implies that the ρ_s^* induced residual stress is stronger than the R H residual zonal flow driven residual stress. This is as expected because the actual level of zonal flow in the turbulent case is higher than in the neoclassical case.

To get a feeling for the importance of the ρ_s^* induced $\langle k_\parallel \rangle$ symmetry breaking driven residual stress relative to the E_r-shear induced $\langle k_\parallel \rangle$ symmetry breaking driven residual stress, the expression for $\Pi_{\parallel,x}^{res}$ in Eq. (18) is estimated numerically for the highest growing mode $(k_{y,max}, \gamma_{max}, \omega_{r,max})$. Here, $k_{y,max}$ is the wave number corresponding to the highest growth γ_{max} and the $\omega_{r,max}$) is the corresponding real frequency. The variation of $\Pi_{\parallel,x}^{res}$ and $\Pi_{\parallel,x}^{E,res}$ with L_n/R is shown in the Fig. 3. It shows that for fixed V'_E the term $\Pi_{\parallel,x}^{res}$ can be dominant over the $\Pi_{\parallel,x}^{E,res}$ term for low values of L_n/R typical to ITBs. Fig. 4 also conveys the same message. Next approximate flow levels generated by these two stresses are evaluated separately. Using the no-slip boundary condition $V(a) = 0$ to the zero net flux equation

$$\chi_\parallel \frac{dV_\parallel}{dx} = \Pi_{\parallel,x}^{res}, \tag{35}$$

yields the intrinsic parallel flow level as

$$V_\parallel(x) = -\int_x^a dx' \frac{\Pi_{\parallel,x}^{res}(x')}{\chi_\parallel(x')}. \tag{36}$$

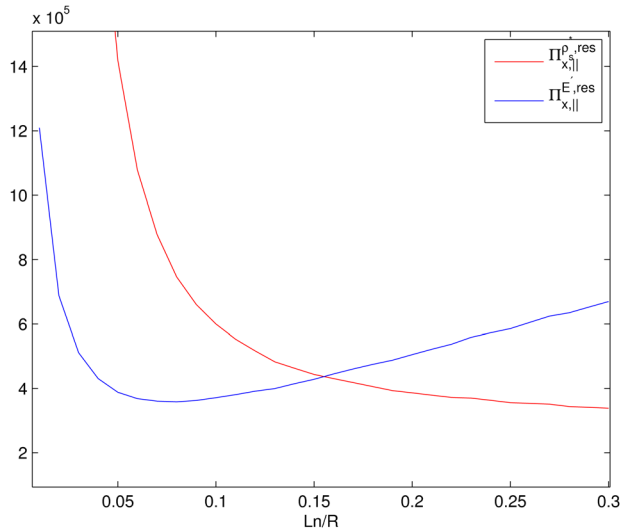

FIG. 3. (Color online) Variation of ρ_s^* induced symmetry breaking driven residual stress $\Pi_{x,\parallel}^{\rho_s^*,res}$ (— curve) and E_r-shear induced symmetry breaking driven residual stress $\Pi_{x,\parallel}^{E',res}$ (— curve) with L_n/R. Stresses are computed corresponding to the highest growing mode for every L_n/R. Parameters: $V'_E = 100\,000\,\mathrm{s}^{-1}$ and other parameters same as in Fig. 1.

This means that the intrinsic parallel flow is determined the synergistic effects of mean profiles embedded in $\Pi_{\parallel,x}^{res}$ and $\chi_\parallel$. To get numbers for $V_\parallel$ we used the following crude approximation

$$|V_\parallel(a/2)| = \frac{\Pi_{\parallel,x}^{res}}{\chi_\parallel}\left(\frac{a}{2}\right), \tag{37}$$

instead of the exact Eq. (36). The typical flow levels thus obtained are shown in Fig. 5. It is accepted that this estimation is far from rigorous. Anyway, Fig. 5 shows that at small L_n/R, the flow driven by ρ_s^* induced $\langle k_\parallel \rangle$ symmetry breaking can become comparable to flow driven by E_r-shear induced by $\langle k_\parallel \rangle$ symmetry breaking.

B. Comparison with parallel polarization stress/flux

The time asymptotic form of the parallel polarization stress can be obtained as

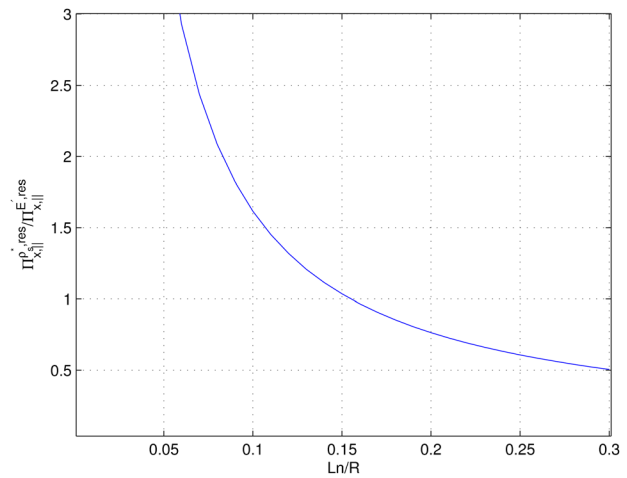

FIG. 4. (Color online) Relative strength of ρ_s^* induced symmetry breaking driven residual stress to E_r-shear induced symmetry breaking driven residual stress vs Ln/R. Parameters: same as in Fig. 3.

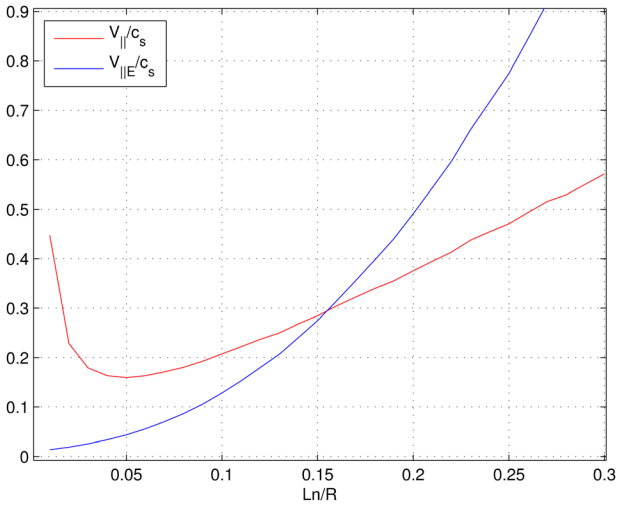

FIG. 5. (Color online) Approximate parallel flow levels evaluated at the mid-minor radius $(a/2)$ by using $V_{\parallel} = -\int_{a/2}^{a} dx(\Pi^{res}_{x,\parallel}/\chi_{\parallel}) = (\Pi^{res}_{x,\parallel}/\chi_{\parallel})(a/2)$. The (—) curve represents ρ_s^* driven flow and the (—) curve represents the E_r' driven flow. This shows that at small L_n/R the ρ_s^* driven flow may be as comparable as E_r' driven flow.

$$\langle \delta v_{polx} \delta v_{\parallel} \rangle = c_s^2 \left(\frac{\rho_s}{L_n}\right)^3 Re \sum_{\vec{k}} \left[\hat{V}'_{\parallel 0} k_x^* k_y - k_x^* k_{\parallel} \left[1 - \frac{\omega_{*pi}}{\omega}\right]\right] |\phi_k|^2, \tag{38}$$

where $k_x = -i\partial_x ln\phi_k$ and $Re(...)$ stands for real part of the expression in $(...)$. The radial wavenumber k_x as obtained from the eigenfunction Eq. (23) is

$$k_x = i\frac{x - \xi_{ks}}{\Delta_{ks}^2} + \frac{|k_y|}{k_y}\frac{\hat{V}'_{\parallel 0}}{2\tau_i \alpha_i}. \tag{39}$$

Now, using the Eq. (39) for k_x, Eq. (24) for the slow mode eigenfrequency and Eq. (23) for the slow mode eigenfunction it is straightforward to show that

$$\langle \delta v_{polx} \delta v_{\parallel} \rangle = \sum_{k_y} c_s^2 \left(\frac{\rho_s}{L_n}\right)^3 k_y^2 s \left[\frac{\hat{V}'_{\parallel 0}}{2\tau_i \alpha_i} \hat{V}'_{\parallel 0} \Delta_{ks} \sqrt{\pi} + \frac{\Delta_{ks}}{2}\sqrt{\pi}\right] |\phi_{0ks}|^2 + O(\epsilon^4), \tag{40}$$

where $\epsilon \sim (\rho_s/L_n) \sim (\omega/\omega_{ci}) \sim (k_{\parallel}/k_y) \ll 1$ in drift wave ordering. Here the diffusive flux appears to be nonlinear, the diffusivity being proportional to the parallel flow shear, due to the fact that real part of the radial wavenumber k_x is dominantly determined by the parallel flow shear for the slow mode. Comparing the leading order residual parallel polarization stress with the ρ_s^* induced symmetry breaking driven residual stress Eq. (21) yields

$$\frac{\Pi^{res}_{\parallel,x}}{\Pi^{pol,res}_{\parallel,x}} = 1. \tag{41}$$

This shows that the ρ_s^* induced symmetry breaking driven residual flux is of the same order as to the leading order parallel polarization flux.

C. Comparison with fluxes driven by turbulence intensity gradient

Now, suppose that there is gradient in the fluctuation intensity introduced by mean profile gradients. We will take the following simple minded expansion of fluctuation intensity $|\phi_{ok}|^2 \equiv \epsilon(x)$

$$\epsilon(x) = \epsilon(0) + x\epsilon(0)' + ... \tag{42}$$

In the following, we will examine the effect of fluctuation intensity gradient on the parallel diffusivity and residual stress separately. Including Eq. (42) in the parallel diffusivity expression yields

$$\chi_{\parallel} = \left(\frac{c_s \rho_s}{L_n}\right)^2 \sum_{k_y} \frac{k_y^2 |k_y| \gamma s}{|\omega|^2} \frac{L_n}{c_s} \left(\epsilon(0) + \epsilon(0)'\xi\right) \Delta\sqrt{\pi}. \tag{43}$$

Comparison of diffusivities for the two cases of ρ_s^* and ϵ' yields

$$\frac{\chi_{\parallel}}{\chi_{\parallel}^{\epsilon'}} = 1. \tag{44}$$

The residual flux takes the form

$$\Pi^{res}_{\parallel,x} = mn_0 \langle \delta v_{Ex} \delta v_{\parallel} \rangle_{res} = mn_0 \left(\frac{c_s \rho_s}{L_n}\right)^2 \sum_{\vec{k}} k_y |k_y| \left[\frac{\gamma}{|\omega|^2} + \frac{\omega_{*pi} 2\gamma\omega_r}{|\omega^2|^2}\right] \langle k_{\parallel} \rangle, \tag{45}$$

where

$$\langle k_{\parallel} \rangle = k_y s \left(\epsilon(0)\xi\Delta\sqrt{\pi} + \epsilon(0)' \left(\Delta^3 \frac{\sqrt{\pi}}{2} + \Delta\xi^2\sqrt{\pi}\right) + ...\right). \tag{46}$$

In case of no spectral shift and no intensity gradient, $\langle k_{\parallel} \rangle$ vanish, and hence, the residual stress vanish. In case of finite spectral shift and uniform turbulence intensity above expression recovers the original well know expression for $\langle k_{\parallel} \rangle$. The $\langle k_{\parallel} \rangle$ may be enhanced or reduced over the uniform intensity case depending upon the sign of the turbulence intensity gradient $\epsilon(0)'$. Also in the case of vanishing spectral shift the sign of $\langle k_{\parallel} \rangle$ is determined by the sign of $\epsilon(0)'$ and the sign of $\langle k_{\parallel} \rangle$ determines the sign of the residual flux $\Pi^{res}_{\parallel,x}$. Comparison of residual stresses equals the comparison of $\langle k_{\parallel} \rangle$ for respective cases. So

$$\frac{\Pi^{res}_{\parallel,x}}{\Pi^{\epsilon',res}_{\parallel,x}} = \frac{\langle k_{\parallel} \rangle_{\rho_s^*}}{\langle k_{\parallel} \rangle_{\epsilon'}} = \frac{\epsilon \rho_s^*}{\epsilon'} = \frac{L_{\epsilon}}{L_n}, \tag{47}$$

where $L_{\epsilon} = \epsilon/\epsilon'$ and $L_n = -n/n'$ are turbulence intensity scale length and density scale length, respectively. Now, it will be interesting to see in which region along the equilibrium profiles these two scale lengths can become comparable. For convenience, we will follow the Ref. 30 and write a few steps for clarity. The turbulence intensity is related to equilibrium profile gradients and so the turbulence intensity

gradient is related to profile curvatures. For example, differentiating the Ficks law for heat flux

$$Q = -\chi_0 \epsilon \frac{\partial T}{\partial x}, \tag{48}$$

for constant heat flux, Q gives the turbulence intensity scale length as

$$L_\epsilon^{-1} = \frac{1}{\epsilon}\frac{\partial \epsilon}{\partial x} = \frac{\epsilon \chi_0}{Q}\frac{\partial^2 T}{\partial x^2}. \tag{49}$$

Then, the flux ratio Eq. (47) turns out to be

$$\frac{\Pi_{\parallel,x}^{res}}{\Pi_{\parallel,x}^{\epsilon',res}} = \frac{\langle k_\parallel \rangle_{\rho_s^*}}{\langle k_\parallel \rangle_{\epsilon'}} = \frac{\epsilon \rho_s^*}{\epsilon'} = \frac{L_\epsilon}{L_n} \propto -\frac{Q}{\chi_0 \epsilon n_0}\frac{n_0'}{T_0''}. \tag{50}$$

This shows that the ρ_s^* effect can be more important at the center of the pedestal or ITB where gradient is stronger than curvature. Whereas turbulence intensity gradient driven parallel momentum flux can be more important at the pedestal/ITB head and foot. Note that this curvature dependence could as well have been shown with particle flux but because electrons are considered adiabatic so it is not attempted. This shows that the ρ_s^* induced symmetry breaking driven residual stress/flux can become comparable to turbulence intensity gradient induced symmetry breaking driven residual stress/flux in strong density gradient region such as ITB or density pedestal in H-mode [see Fig. 6].

IV. RESULTS AND DISCUSSIONS

We presented a clear derivation of the residual stress arising from the $k_\parallel$ symmetry breaking via the shift of the eigenmode off of a mode rational surface, with a fluid system of equations in a simple slab geometry. It shows that the physical process which manifests itself as an asymmetry of the eigenmode in the extended poloidal direction in the ballooning representation or as a radial shift of the eigenmode in a cylindrical formulation, can be captured in a simple slab model in local fluid approximation. This allows one to focus on individual effects for which the global mode structure is not expected to be very important. It is well known that the background density gradient together with fluctuating ion polarization drifts generate a term that accompany plasma vorticity and is proportional to the density gradient. Being one order higher in ρ_s^*, this term is usually not considered in the usual drift wave ordering. We considered the effect of this term using the formulation that we have developed. This term is expected to be important in the regions where the density gradient is large such as H mode pedestal or ITBs. Following are the principal results of this paper.

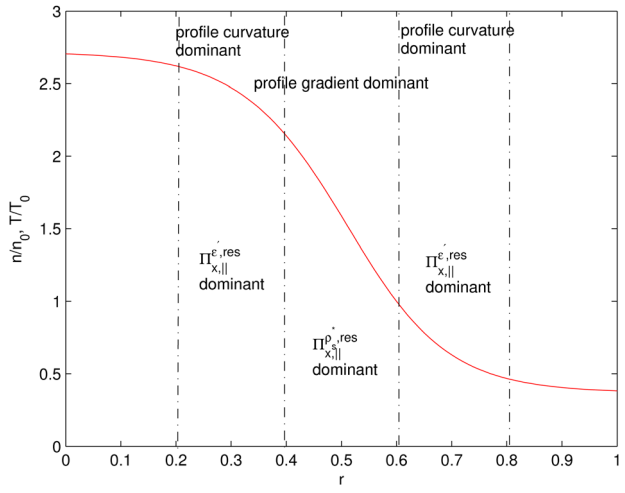

FIG. 6. (Color online) Schematic showing regions of relative importance of ρ_s^* induced symmetry breaking driven residual parallel momentum and turbulence intensity gradient induced symmetry breaking driven parallel residual flux. The vertical dashed-dotted lines are only for roughly highlighting the regoins where the respective fluxes are dominating.

- The new term considered here leads to the formation of residual parallel Reynolds stress, via finite ρ_s^* driven parallel symmetry breaking. The mode structure shifts radially off of a resonance surface. Thus, when the effects of all neighbouring modes, which are similarly shifted are considered, it generates a net $k_\parallel$. This then gives rise to a net Reynolds stress, which transport momentum even in the absence of any net momentum. Comparing this term with the more conventional $E \times B$ shear driven residual stress term, we find that the ratio is basically given by the ratio:

$$\frac{\Pi_{\parallel,x}^{res}}{\Pi_{\parallel,x}^{E,res}} \propto \rho_s^{*2}\frac{\Omega_i}{V_{E0}'}.$$

  Note that in the usual gyrokinetic ordering $\frac{\rho}{L_n} \sim \frac{\omega}{\Omega_i}$, and the condition for the shear suppression to become important is roughly $\omega/V_{E0}' \sim 1$. Which suggests that the term that we introduce here is an order higher than the $E \times B$ shear driven term in terms of ρ_s^*. While it is true that a sharper density gradient will reduce this difference, the sharper density gradients are also usually accompanied by deeper E_r wells.
  Nevertheless, the term is important for completeness. It needs to be included in a detailed analysis. It also has explicit density gradient dependence. As such, it complements the part of the $E \times B$ shear that comes from the profile gradients in the radial force balance.
- V_E' may also be interpreted as zonal flow shear which is generated by polarization current. The ρ_s^* effect also originates from the polarization current. The zonal shear level can be estimated via mixing length as being roughly proportional to ρ_s^*, so that ρ_s^* effect introduced here, can be thought of as being linked to the zonal $E \times B$ shear induced symmetry breaking. The ρ_s^* induced residual stress is expected to be stronger than the R H neoclassical residual zonal flow shear induced residual stress.
- Comparing ρ_s^* driven residual stress with the parallel polarization stress shows that they are of the same order. In particular

$$\frac{\Pi_{\parallel,x}^{res}}{\Pi_{\parallel,x}^{pol,res}} = 1.$$

for the slow mode branch.

- Similarly comparison with turbulence gradient induced residual stress shows that

$$\frac{\Pi_{\parallel,x}^{res}}{\Pi_{\parallel,x}^{\epsilon',res}} = \frac{\langle k_\parallel \rangle_{\rho_s^*}}{\langle k_\parallel \rangle_{\epsilon'}} = \frac{\epsilon \rho_s^*}{\epsilon'} = \frac{L_\epsilon}{L_n},$$

where L_ϵ and L_n are turbulence intensity gradient length scale and density gradient length scale, respectively. L_ϵ is decided by the profile curvatures. In the sharp gradient region L_n is small, curvature is weak and so L_ϵ is large. This means that the ρ_s^* driven residual stress overtakes the turbulence intensity inhomogenity driven residual stress in the sharp density gradient and weak curvature regions along the mean profiles. In contrast, near the "corners," where curvature is large, the intensity gradient term will be larger.

- For homogeneous turbulence intensity, the parallel momentum diffusivity is found not to show any response to this new ρ_s^* effect reported here. This is because the momentum diffusivity does not depend on the broken symmetry of the eigenfunction. However, broken symmetry of the eigenfunction together with turbulence intensity inhomogenity does renormalize the parallel momentum diffusivity [e.g., see Eq. (43)].

ACKNOWLEDGMENTS

This work is partly supported by the French Agence nationale de la recherche, contract ANR JCJC 0403 01.

[1]G. R. Mckee, P. Gohil, D. Schlossberg, J. Boedo, K. Burrell, J. deGrassie, R. Groebner, R. Moyer, C. Petty, T. Rhodes, L. Schmitz, M. Shafer, W. Solomon, M. Umansky, G. Wang, A. White, and X. Xu, Nucl. Fusion **49**, 115016 (2009).
[2]H. Biglari, P. H. Diamond, and P. W. Terry, Phys. Fluids B **2**, 1 (1990).
[3]T. S. Hahm, Phys. Plasmas **1**, 2940 (1994).
[4]T. S. Hahm and K. H. Burrell, Phys. Plasmas **2**, 1648 (1995).
[5]T. S. Hahm and K. H. Burrell, Plasma Phys. Controlled Fusion **38**, 1427 (1996).
[6]J. Rice, R. Boivin, P. Bonoli, J. Goetz, R. Granetz, M. Greenwald, I. Hutchinson, E. Marmar, G. Schilling, J. Snipes, S. Wolfe, S. Wukitch, C. Fiore, J. Irby, D. Mossessian, and M. Porkolab, Nucl. Fusion **41**, 277 (2001).
[7]E. J. Strait, T. S. Taylor, A. D. Turnbull, J. R. Ferron, L. L. Lao, B. Rice, O. Sauter, S. J. Thompson, and D. Wróblewski, Phys. Rev. Lett. **74**, 2483 (1995).
[8]A. M. Garofalo, A. D. Turnbull, M. E. Austin, J. Bialek, M. S. Chu, K. J. Comer, E. D. Fredrickson, R. J. Groebner, R. J. La Haye, L. L. Lao, E. A. Lazarus, G. A. Navratil, T. H. Osborne, B. W. Rice, S. A. Sabbagh, J. T. Scoville, E. J. Strait, and T. S. Taylor, Phys. Rev. Lett. **82**, 3811 (1999).
[9]L.-J. Zheng, M. Kotschenreuther, and M. S. Chu, Phys. Rev. Lett. **95**, 255003 (2005).
[10]L. J. Zheng, M. T. Kotschenreuther, and J. W. V. Dam, Phys. Plasmas **17**, 056104 (2010).
[11]T. C. Hender, J. C. Wesley, J. Bialek, A. Bondeson, A. H. Boozer, R. J. Buttery, A. Garofalo, T. P. Goodman, R. S. Granetz, Y. Gribov, O. Gruber, M. Gryaznevich, G. Giruzzi, S. Gnter, N. Hayashi, P. Helander, C. C. Hegna, D. F. Howell, D. A. Humphreys, G. T. A. Huysmans, A. W. Hyatt, A. Isayama, S. C. Jardin, Y. Kawano, A. Kellman, C. Kessel, H. R. Koslowski, R. J. L. Haye, E. Lazzaro, Y. Q. Liu, V. Lukash, J. Manickam, S. Medvedev, V. Mertens, S. V. Mirnov, Y. Nakamura, G. Navratil, M. Okabayashi, T. Ozeki, R. Paccagnella, G. Pautasso, F. Porcelli, V. D. Pustovitov, V. Riccardo, M. Sato, O. Sauter, M. J. Schaffer, M. Shimada, P. Sonato, E. J. Strait, M. Sugihara, M. Takechi, A. D. Turnbull, E. Westerhof, D. G. Whyte, R. Yoshino, H. Zohm, D. ITPA MHD, and M. C. T. Group, Nucl. Fusion S128 (2007).
[12]R. J. Hawryluk, D. J. Campbell, G. Janeschitz, P. Thomas, R. Albanese, R. Ambrosino, C. Bachmann, L. Baylor, M. Becoulet, I. Benfatto, J. Bialek, A. Boozer, A. Brooks, R. Budny, T. Casper, M. Cavinato, J.-J. Cordier, V. Chuyanov, E. Doyle, T. Evans, G. Federici, M. Fenstermacher, H. Fujieda, K. Gal, A. Garofalo, L. Garzotti, D. Gates, Y. Gribov, P. Heitzenroeder, T. Hender, N. Holtkamp, D. Humphreys, I. Hutchinson, K. Ioki, J. Johner, G. Johnson, Y. Kamada, A. Kavin, C. Kessel, R. Khayrutdinov, G. Kramer, A. Kukushkin, K. Lackner, I. Landman, P. Lang, Y. Liang, J. Linke, B. Lipschultz, A. Loarte, G. Loesser, C. Lowry, T. Luce, V. Lukash, S. Maruyama, M. Mattei, J. Menard, M. Merola, A. Mineev, N. Mitchell, E. Nardon, R. Nazikia, B. Nelson, C. Neumeyer, J.-K. Park, R. Pearce, R. Pitts, A. Polevoi, A. Portone, M. Okabayashi, P. Rebut, V. Riccardo, J. Roth, S. Sabbagh, G. Saibene, G. Sannazzaro, M. Schaffer, M. Shimada, A. Sen, A. Sips, C. Skinner, P. Snyder, R. Stambaugh, E. Strait, M. Sugihara, E. Tsitrone, J. Urano, M. Valovic, M. Wade, J. Wesley, R. White, D. Whyte, S. Wu, M. Wykes, and L. Zakharov , Nucl. Fusion **49**, 065012 (2009).
[13]R. Hemsworth, H. Decamps, J. Graceffa, B. Schunke, M. Tanaka, M. Dremel, A. Tanga, H. D. Esch, F. Geli, J. Milnes, T. Inoue, D. Marcuzzi, P. Sonato, and P. Zaccaria, Nucl. Fusion **49**, 045006 (2009).
[14]N. Holtkamp, *Proceedings of 22nd International Conference on Fusion Energy*, Geneva Switzerland, 2008 (IAEA, Viena) OV/2-1.
[15]J. E. Rice,A. Ince-Cushman, J. deGrassie, L.-G. Eriksson, Y. Sakamoto, A. Scarabosio, A. Bortolon, K. Burrell, B. Duval,C. Fenzi-Bonizec, M. Greenwald, R. Groebner, G. Hoang, Y. Koide, E. Marmar, A. Pochelon, and Y. Podpaly, Nucl. Fusion **47**, 1618 (2007).
[16]J. E. Rice, E. S. Marmar, P. T. Bonoli, R. S. Granetz, M. J. Greenwald, A. E. Hubbard, J. W. Hughes, I. H. Hutchinson, J. H. Irby, B. Labombard, W. D. Lee, Y. Lin, D. Mossessian, J. A. Snipes, S. M. Wolfe, and S. J. Wukitch, Fusion Sci. Technol. **51**, 288 (2007).
[17]W. M. Solomon, K. H. Burrell, A. M. Garofalo, S. M. Kaye, R. E. Bell, A. J. Cole, J. S. deGrassie, P. H. Diamond, T. S. Hahm, G. L. Jackson, M. J. Lanctot, C. C. Petty, H. Reimerdes, S. A. Sabbagh, E. J. Strait, T. Tala, and R. E. Waltz, Phys. Plasmas **17**, 056108 (2010).
[18]P. H. Diamond, C. J. McDevitt, Ö. D. Gürcan, T. Hahm, W. X. Wang, E. Yoon, I. Holod, Z. Lin, V. Naulin, and R. Singh, Nucl. Fusion **49**, 045002 (2009).
[19]P. H. Diamond, C. J. McDevitt, Ö. D. Gürcan, T. S. Hahm, and V. Naulin, Phys. Plasmas **15**, 012303 (2008).
[20]N. Mattor and P. H. Diamond, Phys. Fluids **31**, 1180 (1988).
[21]W. X. Wang, T. S. Hahm, S. Ethier, G. Rewoldt, W. W. Lee, W. M. Tang, S. M. Kaye, and P. H. Diamond, Phys. Rev. Lett. **102**, 035005 (2009).
[22]S. D. Scott, P. H. Diamond, R. J. Fonck, R. J. Goldston, R. B. Howell, K. P. Jaehnig, G. Schilling, E. J. Synakowski, M. C. ZarnstorA, C. E. Bush, E. Fredrickson, K. W. Hill, A. C. Janos, D. K. Mansfield, D. K. Owens, H. Park, G. Pautasso, A. T. Ramsey, J. Schivell, G. D. Tait, W. M. Tang, and G. Taylor, Phys. Rev. Lett. **64**, 531 (1990).
[23]I. Holod and Z. Lin, Phys. Plasmas **15**, 092302 (2008).
[24]T. S. Hahm, P. H. Diamond, O. D. Gurcan, and G. Rewoldt, Phys. Plasmas **14**, 072302 (2007).
[25]A. G. Peeters, C. Angioni, and D. Strintzi, Phys. Rev. Lett. **98**, 265003 (2007).
[26]Ö. D. Gürcan, P. H. Diamond, and T. S. Hahm, Phys. Rev. Lett. **100**, 135001 (2008).
[27]N. Kluy, C. Angioni, Y. Camenen, and A. G. Peeters, Phys. Plasmas **16**, 122302 (2009).
[28]E. S. Yoon and T. S. Hahm, Nucl. Fusion **50**, 064006 (2010).
[29]C. J. McDevitt and P. H. Diamond, Phys. Plasmas **16**, 012301 (2009).
[30]O. D. Grcan, P. H. Diamond, P. Hennequin, C. J. McDevitt, X. Garbet, and C. Bourdelle, Phys. Plasmas **17**, 112309 (2010).
[31]Y. Camenen, A. G. Peeters, C. Angioni, F. J. Casson, W. A. Hornsby, A. P. Snodin, and D. Strintzi, Phys. Rev. Lett. **102**, 125001 (2009).
[32]Y. Camenen, A. G. Peeters, C. Angioni, F. J. Casson, W. A. Hornsby, A. P. Snodin, and D. Strintzi, Phys. Plasmas **16**, 062501 (2009).
[33]J. Weiland, R. Singh, H. Nordman, P. Kaw, A. Peeters, and D. Strinzi, Nucl. Fusion **49**, 065033 (2009).
[34]Ö. D. Gürcan, P. H. Diamond, T. S. Hahm, and R. Singh, Phys. Plasmas **14**, 042306 (2007).
[35]M. Yoshida, Y. Kamada, H. Takenaga, Y. Sakamoto, H. Urano, N. Oyama, and G. Matsunaga, Phys. Rev. Lett. **100**, 105002 (2008).
[36]D. Whyte, A. Hubbard, J. Hughes, B. Lipschultz, J. Rice, E. Marmar, M. Greenwald, I. Cziegler, A. Dominguez, T. Golfinopoulos, N. Howard, L. Lin, R. McDermott, M. Porkolab, M. Reinke, J. Terry, N. Tsujii, S. Wolfe, S. Wukitch, Y. Lin, and the Alcator C-Mod Team, Nucl. Fusion **50**, 105005 (2010).

[37]J. E. Rice, J. W. Hughes, P. H. Diamond, Y. Kosuga, Y. A. Podpaly, M. L. Reinke, M. J. Greenwald, O. D. Gurcan, T. S. Hahm, A. E. Hubbard, E. S. Marmar, C. J. McDevitt, and D. G. Whyte, Phys. Rev. Lett. **106**, 215001 (2011).
[38]K. Ida, M. Yoshinuma, K. Nagaoka, M. Osakabe, S. Morita, M. Goto, M. Yokoyama, H. Funaba, S. Murakami, K. Ikeda, H. Nakano, K. Tsumori, Y. Takeiri, O. Kaneko, and L. experiment group, Nucl. Fusion **50**, 064007 (2010).
[39]W. X. Wang, P. H. Diamond, T. S. Hahm, S. Ethier, G. Rewoldt, and W. M. Tang, Phys. Plasmas **17**, 072511 (2010).
[40]F. J. Casson, A. G. Peeters, Y. Camenen, W. A. Hornsby, A. P. Snodin, D. Strintzi, and G. Szepesi, Phys. Plasmas **16**, 092303 (2009).
[41]W. X. Wang, T. S. Hahm, S. Ethier, L. E. Zakharov, and P. H. Diamond, Phys. Rev. Lett. **106**, 085001 (2011).
[42]R. Singh, R. Ganesh, R. Singh, P. Kaw, and A. Sen, Nucl. Fusion **51**, 013002 (2011).
[43]C. J. McDevitt, P. Diamond, O. Gurcan, and T. Hahm, Phys. Plasmas **16**, 052302 (2009).
[44]C. J. McDevitt, P. Diamond, and O. Gurcan, Phys. Rev. Lett. **103**, 205003 (2009).
[45]Z. Yan, M. Xu, C. H. P. H. Diamond, S. H. Muller, G. R. Tyan, and J. H. Yu, Phys. Rev. Lett. **104**, 065002 (2010).
[46]S. H. Müller, J. A. Boedo, K. H. Burrell, J. S. deGrassie, R. A. Moyer, D. L. Rudakov, and W. M. Solomon, Phys. Rev. Lett. **106**, 115001 (2011).
[47]S. Hamaguchi and W. Horton, Phys. Fluids B **4**, 319 (1992).
[48]N. Mattor and P. H. Diamond, Phys. Fluids **31**, 1180 (1988).
[49]L. Bai, A. Fukuyama, and M. Uchida, Phys. Plasmas **5**, 989 (1998).
[50]D. H. E. Dubin, J. A. Krommes, C. Oberman, and W. W. Lee, Phys. Fluids **26**, 3524 (1983).
[51]A. Brizard, Phys. Fluids B **4**, 1213 (1992).
[52]M. N. Rosenbluth and F. L. Hinton, Phys. Rev. Lett. **80**, 724 (1998).